

Determining the Refractive Index of Human Hemoglobin Solutions by Kramers-Kronig Relations with an Improved Absorption Model

JONAS GIENGER^{1,*}, HERMANN GROSS¹, JÖRG NEUKAMMER¹, AND MARKUS BÄR¹

¹Physikalisch-Technische Bundesanstalt (PTB), Abbestraße 2–12, 10587 Berlin, Germany

*Corresponding author: jonas.gienger@ptb.de

Compiled November 8, 2017

The real part of the refractive index (RI) of aqueous solutions of human hemoglobin is computed from their absorption spectra in the wavelength range 250 nm–1100 nm using the Kramers-Kronig (KK) relations and the corresponding uncertainty analysis is provided. The strong ultraviolet (UV) and infrared absorbance of the water outside this spectral range were taken into account in a previous study employing KK relations. We improve these results by including the concentration dependence of the water absorbance as well as by modeling the deep UV absorbance of hemoglobin's peptide backbone. The two free parameters of the model for the deep UV absorbance are fixed by a global fit.

© 2016 Optical Society of America. One print or electronic copy may be made for personal use only. Systematic reproduction and distribution, duplication of any material in this paper for a fee or for commercial purposes, or modifications of the content of this paper are prohibited.

OCIS codes: 000.1430 *Biology and medicine*; 000.3860 *Mathematical methods in physics*; 120.4530 *Optical constants*; 260.2030 *Dispersion*; 300.1030 *Absorption*

<http://dx.doi.org/10.1364/AO.55.008951>

1. INTRODUCTION

The optical properties of biological cells and tissues have been subject to research for many decades. Refractometry in cells is used, e. g., for protein detection [1]. Recently, the refractive index (RI) or RI distribution of cells has been measured by phase microscopy [2], holographic techniques [3], absorption cytometry [4] or optical tomography [5]. From such measurements, the dry mass or concentrations of proteins in the cell can be derived, provided the relation to the optical properties is known.

Analysis of blood samples includes the determination of the quantities of the so called complete blood count (CBC), one of the most frequently performed measurements in laboratory medicine. Besides the concentrations of red blood cells (RBCs, erythrocytes), white blood cells and platelets, an important indicator for diseases, e. g., anemia, is the mean cellular volume (MCV) of red blood cells. Besides the calculation of the MCV as ratio of the hematocrit value and the RBC concentration, flow-cytometric detection of light scattering by RBCs is being used for more than three decades to determine the volume and hemoglobin content of individual cells [6, 7] at a throughput in the range of 1000 events per second. Of course, a detailed knowledge of the cells' refractive index is required for this. Since RBCs are mainly composed of the protein complex hemoglobin (Hb), which is dissolved in water at an average in-

tracellular concentration of typically 340 g L⁻¹ for healthy persons, the knowledge of the Hb RI is of crucial importance to reliably calculate RBC volume and Hb content.

Within the blood of a single person, the intracellular Hb concentration fluctuates among the individual RBCs, with a coefficient of variation around 6–8% [5, 6]. Because of the significant influence of this variation, it does not suffice to know the RI of hemoglobin solutions at the mean concentration, but the dependence of the RI on the concentration has to be specified.

The absorption spectra of Hb solutions were measured with high accuracy over a wide range of wavelengths and are known for several decades. In contrast, measurements of their refractive index, especially at physiologically relevant high concentrations, are challenging and have only been presented as late as 2005 for a wide spectral range [8]. However, these data have much larger measurement uncertainties than the corresponding absorption spectra, such that the real part of the complex refractive index is less accurately known than its imaginary part, the absorbance.

As a remedy several authors [9, 10] suggested to employ Kramers-Kronig (KK) relations in order to obtain the real part of the RI directly from accurate measurements of absorption spectra, i. e., the imaginary part of the RI as a function of wavelength. However, this is a non-trivial task due to the finite wavelength range of the measured spectra and the global, long-ranged char-

acter of the KK relations which yield the real part of the RI as an integral transformation of the imaginary part. In this paper, we supplement and extend the literature spectra [8] with an absorption model for proteins towards the UV. As a result we obtain RIs that are in better agreement with results obtained by reflectance measurements for oxyhemoglobin solutions [11]. Furthermore we obtain results for the RI of deoxyhemoglobin and give the *refractive increment*, i. e., the slope of the RI with respect to concentration for the first time. We also extend the previous treatment by considering the measurement uncertainties of the obtained RIs. These uncertainties result from the propagation of the uncertainties of the measured absorption spectra [8] and the refractive index data obtained by reflectance measurements [11], to which we fit the two free parameters of the deep UV absorption model. The mathematical model for the absorption spectra and related method are presented in sections 2 and 3. Our approach can be applied to any variant of hemoglobin. Section 2A describes the imaginary part of the RI of a Hb solution in dependence on concentration. KK relations are used in section 2B to obtain an expression for the real part of the solution's RI. A model for the deep UV absorbance of hemoglobin is proposed in section 2B as well. Section 2C describes the fitting of the two free model parameters to the literature data for the real part of the RI. In section 3, we apply the analysis to experimental data for oxygenated and deoxygenated hemoglobin, respectively. The significance of the results is discussed and a comparison to previous KK-analyses is made. In section 4, we summarize our findings.

Terminology

Oxygenated hemoglobin is often abbreviated as "HbO₂" while deoxygenated hemoglobin is usually abbreviated as "Hb". In order to simplify the notation we will use the term "Hb" for hemoglobin in general, specifying the hemoglobin variant only if relevant.

The RI of Hb solutions complex-valued. For the sake of brevity, we refer to the real part of the RI by "real RI" and to the imaginary part of the RI by "imaginary RI". This shall not imply that the RI is purely real or imaginary.

2. MATERIALS AND METHODS

A. Absorption Spectra: Imaginary Part of Refractive Index

The Hb absorption spectra in the wavelength range [250,1100] nm reported in [8] were used in our calculations. These data were measured for Hb solutions produced from human erythrocytes by repeated freezing and thawing followed by centrifugation of the membrane components. These homogeneous solutions did thus contain all the constituents of human erythrocytes, except for the membranes (thickness less than a few 10 nm, volume fraction less than a few % [6, 12, 13]). We further use experimental data for pure Hb solutions to supplement the absorbance data in the wavelength range 228 nm–250 nm [14].

Other researchers [9, 10] have previously relied on the data compiled from various sources by Prahl [15]. However, since not all of the compiled sources used human hemoglobin, these data are not used here.

A.1. Literature Data

The literature absorption spectra we use in our calculations are expressed in terms of the inverse absorption length $\mu_a(\lambda)$ at a given mass concentration c or the molar extinction coefficient

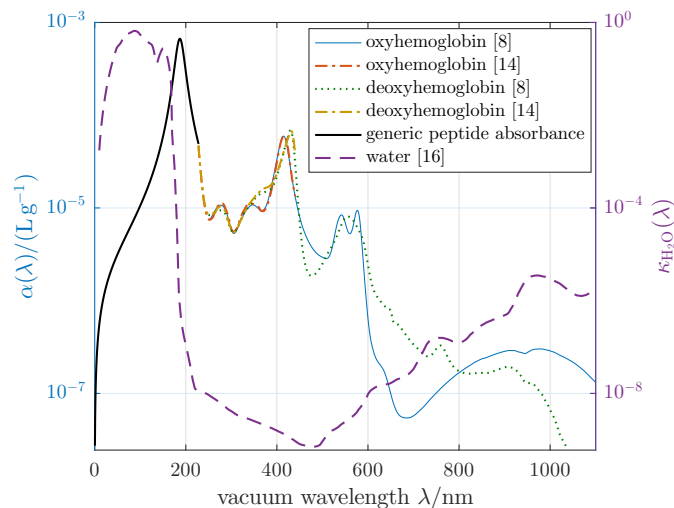


Fig. 1. Imaginary refractive increment $\alpha(\lambda)$ of hemoglobin in aqueous solutions (left axis, solid and dash-dotted lines). Experimental data are taken from [8] (corrected for H₂O absorbance) and [14]. A Lorentzian peak models the deep UV absorbance of the peptide backbone (left axis, solid black line). Imaginary RI $\kappa_{\text{H}_2\text{O}}(\lambda)$ of water (right axis, dashed line) [16]. Note that the quantities α , $\kappa_{\text{H}_2\text{O}}$ have different units and scaling of y -axes. To compare the numerical values of α and $\kappa_{\text{H}_2\text{O}}$, one needs to multiply α by the respective concentration of the RBC, e. g., $c_{\text{Hb}} = 340 \text{ g L}^{-1}$, cf. Eq. (5). Spline interpolation was applied to obtain a step width of 1 nm.

$\varepsilon_M(\lambda)$, where λ is the vacuum wavelength of the light. The latter implies that the Lambert-Beer law holds, which is the case for Hb at physiological ($c \approx 300 \text{ g L}^{-1}$) or lower concentrations [8]. Instead of $\mu_a(\lambda)$ or $\varepsilon_M(\lambda)$, we express the absorption spectra in terms of the imaginary part of the complex RI

$$n(\lambda) = n(\lambda) + i\kappa(\lambda) \quad (1)$$

of the solution. Here n, κ are positive real functions. The conversion rule is

$$\kappa(\lambda) = \frac{\mu_a(\lambda) \lambda}{4\pi} = \frac{\ln 10 \varepsilon_M(\lambda) c \lambda}{4\pi M}. \quad (2)$$

The data on the molar extinction coefficient $\varepsilon_M(\lambda)$ from [14] are converted to $\kappa(\lambda)$, using the molar mass of the Hb tetramer $M = 64458 \text{ g mol}^{-1}$ [17].

A.2. Total Absorbance of Hb Solutions and Erythrocytes

In the spectral range of $\lambda \in [250, 1100]$ nm the strongest absorption of light by RBCs and hence of blood is caused by Hb. Water has a fairly low absorption coefficient in this region (cf. Fig. 1) and other RBC components contained in the cytosol (e. g., other proteins, sugars, ions) exhibit rather low concentrations. We thus consider a two-component system, i. e.,

1. the solvent, or simply "Water" (H₂O), occupying a volume $V_{\text{H}_2\text{O}}$ and
2. the absorbing solute, or simply "Hemoglobin" (Hb), denoting everything else contained in the erythrocyte cytosol and occupying a volume V_{Hb} . The solute is treated as pure Hb for its other physical properties, such as molar mass and density.

Let the volume fraction occupied by Hb molecules be $\phi = V_{\text{Hb}}/(V_{\text{H}_2\text{O}} + V_{\text{Hb}})$ and the volume fraction occupied by water molecules $1 - \phi = V_{\text{H}_2\text{O}}/(V_{\text{H}_2\text{O}} + V_{\text{Hb}})$. Since the Lambert-Beer law holds, we make the following ansatz for the total imaginary RI (absorbance) of the solution

$$\kappa(\lambda) = \phi \kappa_{\text{Hb}}(\lambda) + (1 - \phi) \kappa_{\text{H}_2\text{O}}(\lambda), \quad (3)$$

where $\kappa_{\text{H}_2\text{O}}(\lambda)$ is the absorbance of pure water and $\kappa_{\text{Hb}}(\lambda)$ is the absorbance of “pure hemoglobin in aqueous solution”. It should be noted that κ_{Hb} is not equal to the imaginary RI of a crystal of pure hemoglobin as is revealed by comparison with data for the complex dielectric function of thin Hb films [18]. Eq. (3) is similar to the ansatz in [10], where, however, the authors did not include the prefactor $1 - \phi$ for the water absorbance, which results in a relevant difference as shown later. This *excluded volume* effect, i. e., the fact that there is less water in a solution of higher Hb concentration is essential and must be taken into account since the volume fractions of Hb can be as high as 26% or more.

The Hb volume fraction is related to the concentration by

$$\phi = \frac{c_{\text{Hb}}}{\rho_{\text{Hb}}}, \quad (4)$$

where ρ_{Hb} is the mass density of a hypothetical solution containing 100% Hb and 0% H_2O . Both, $\kappa_{\text{Hb}}(\lambda)$ and ρ_{Hb} are coefficients in a linear interpolation of spectra and density that holds at least up to physiologically high concentrations. A value of $\rho_{\text{Hb}} = 1330 \text{ g L}^{-1}$ for proteins is given in [1], independent of the type of protein. A normal physiological intra-erythrocyte Hb concentration of 340 g L^{-1} thus corresponds to a volume fraction of $\phi \approx 0.26$ or 26%.

Then the term for the absorbance contribution of Hb, $\phi \kappa_{\text{Hb}}(\lambda)$, becomes

$$\phi \kappa_{\text{Hb}}(\lambda) = c_{\text{Hb}} \frac{\kappa_{\text{Hb}}(\lambda)}{\rho_{\text{Hb}}} \stackrel{\text{def. } \alpha(\lambda)}{=} c_{\text{Hb}} \alpha(\lambda), \quad (5)$$

where $\alpha(\lambda)$ is Hb’s concentration-specific increment of the imaginary RI, or the *imaginary refractive increment*. Since the Hb concentration c_{Hb} is measured in g L^{-1} , the unit for α is L g^{-1} . Eq. (3) becomes

$$\kappa(\lambda) = c_{\text{Hb}} \alpha(\lambda) + \left(1 - \frac{c_{\text{Hb}}}{\rho_{\text{Hb}}}\right) \kappa_{\text{H}_2\text{O}}(\lambda). \quad (6)$$

Eq. (6) together with Eq. (2) and Eq. (3) allows to compute the imaginary refractive increment $\alpha(\lambda)$ from a measurement of the inverse absorption length $\mu_a^*(\lambda)$ of a solution at known concentration c_{Hb}^* as

$$\begin{aligned} \alpha(\lambda) &= \frac{1}{c_{\text{Hb}}^*} [\kappa^*(\lambda) + (\phi^* - 1) \kappa_{\text{H}_2\text{O}}(\lambda)] \\ &= \frac{1}{c_{\text{Hb}}^*} \frac{\lambda}{4\pi} \left[\mu_a^*(\lambda) + \left(\frac{c_{\text{Hb}}^*}{\rho_{\text{Hb}}} - 1 \right) \mu_{a,\text{H}_2\text{O}}(\lambda) \right], \end{aligned} \quad (7)$$

where the asterisk * denotes experimental data. The inverse absorption length of water $\mu_{a,\text{H}_2\text{O}}(\lambda)$ is known to high accuracy over a large spectral range $\lambda \in [10 \text{ nm}, 10 \text{ m}]$ [16]. Hence this formula allows to correct for the water absorption, which is important in the infrared (IR), where Hb absorbs only weakly.

B. Real Part of Refractive Index by Kramers-Kronig Relations

B.1. Literature Data

The most complete experimental measurement of the wavelength-dependent real RI of Hb solutions to date was presented in [8, 11]. Here, $n(\lambda)$ was determined via measurements of the spectral reflectance $R(\lambda)$ at an interface between air and Hb solution at normal incidence. The reflectance at normal incidence is connected to the complex refractive index by the Fresnel equation

$$R(\lambda) = \left| \frac{n(\lambda) - 1}{n(\lambda) + 1} \right|^2 = \frac{(n(\lambda) - 1)^2 + \kappa(\lambda)^2}{(n(\lambda) + 1)^2 + \kappa(\lambda)^2}, \quad (8)$$

which is easily solved for $n(\lambda)$ when $\kappa(\lambda)$ is known or when it can be neglected because $\kappa(\lambda) \ll n(\lambda) - 1$.

In [11] measurements at different concentrations were analyzed. A linear-affine dependence of the real RI on the concentration was found and the result was expressed as

$$n(\lambda) = n_{\text{H}_2\text{O}}(\lambda) [1 + c_{\text{Hb}} \beta(\lambda)]. \quad (9)$$

Here $\beta(\lambda)$ is the concentration-specific increment of the real RI relative to the water RI.

B.2. Kramers-Kronig Relations

The complex refractive index is a linear, causal response-function to an incident wave. Hence its real and imaginary part are related by KK relations. Expressed in terms of wavelengths, the KK relations for the complex RI read

$$n(\lambda) - 1 = \mathcal{K}[\kappa](\lambda) := -\frac{2}{\pi} \int_0^\infty \frac{\lambda'}{\Lambda} \frac{\lambda}{\Lambda^2 - \lambda'^2} \kappa(\Lambda) d\Lambda, \quad (10)$$

$$\kappa(\lambda) = \mathcal{K}^{-1}[n](\lambda) = +\frac{2}{\pi} \int_0^\infty \frac{\lambda'}{\Lambda^2 - \lambda'^2} n(\Lambda) d\Lambda, \quad (11)$$

where Eq. (10) also defines the integral transform \mathcal{K} in general. The symbol $:=$ denotes a definition and the symbol f denotes the Cauchy principal value integral.

Applying Eq. (10) formally to the ansatz for the absorption of the Hb solution Eq. (6), we obtain

$$n(\lambda) - 1 = c_{\text{Hb}} G(\lambda) + \left(1 - \frac{c_{\text{Hb}}}{\rho_{\text{Hb}}}\right) (n_{\text{H}_2\text{O}}(\lambda) - 1), \quad (12)$$

where $G(\lambda) := \mathcal{K}[\alpha](\lambda)$ is the transformed spectrum (cf. Eq. (10)). This formal transformation of the absorption results in an equation for the real RI of the Hb solution

$$\begin{aligned} n(\lambda) &= n_{\text{H}_2\text{O}}(\lambda) + c_{\text{Hb}} \left[G(\lambda) - \frac{n_{\text{H}_2\text{O}}(\lambda) - 1}{\rho_{\text{Hb}}} \right] \\ &\stackrel{\text{def. } B(\lambda)}{=} n_{\text{H}_2\text{O}}(\lambda) + c_{\text{Hb}} B(\lambda). \end{aligned} \quad (13)$$

The linear-affine dependence of $n(\lambda)$ on c_{Hb} in Eq. (13) is in agreement with experimental findings [11] (cf. Eq. (9)). In Eq. (6), we have formally split off the water absorption, such that $n_{\text{H}_2\text{O}}(\lambda)$ contributes to the background in the dispersion relations of the Hb solutions (cf. Eq. (13)). Since the real RI of water – unlike the real RI of Hb – is known to high accuracy, this provides valuable additional information compared to the application of the KK-transform only to the measured absorption spectrum of a Hb solution in the visible and near UV/IR range that was presented in [9]. This idea was already presented in [10]. However, due to our different ansatz for the absorption, where we take into account the *excluded water volume*, we obtain a different result for $B(\lambda)$ with an additional

term $(n_{\text{H}_2\text{O}}(\lambda) - 1)/\rho_{\text{Hb}}$ for the concentration dependence. We discuss the differences between the results obtained in [9], [10] and the result with our improved model in section 3B.

For numerical values of $n_{\text{H}_2\text{O}}(\lambda)$, we use a four-term Sellmeier formula that is accurate to at least five decimal places [19].

B.3. Additional Spectral Information Outside the Measured Range

The KK relations provide a formal tool to derive results like Eq. (13). However, their application has a well known problem for the numerical evaluation: They are global integral transforms that require the knowledge of real or imaginary RI at all wavelengths $\lambda \in [0, \infty]$, which is practically impossible. Although the integral kernel in Eq. (10) is decaying with increasing distance from the pole at $\Lambda = \lambda$, it is long-ranged. Hence, one cannot simply cut off the integration domain, i. e., use a finite dataset.

Water is transparent to visible light and its main regions of absorption lie in the UV and the IR (Fig. 1). Due to these absorption bands water has a RI significantly different from 1, even in the transparent regions and exhibits normal dispersion, i. e., $n(\lambda)$ decreases with λ . This implies that neglecting such contributions in the KK relations may lead to inaccurate results. We will now describe the absorption features of Hb below 250 nm by a mathematical model and include them in our expression for the real RI.

In addition to the known absorption spectrum (Fig. 1) with strong absorption in the vicinity of the Soret band at 420 nm, Hb has an even stronger absorption peak in the deep UV. This feature stems from the peptide bonds forming the backbone of any polypeptide or protein, including the protein complex hemoglobin and is characteristic for polypeptides and proteins. The corresponding extinction coefficient curves $\varepsilon(\lambda)$ are similar among a variety of proteins and the absorbance maximum is typically located at $\lambda = 187$ nm [20, 21].

This peptide-peak must be accounted for to perform a proper KK analysis, but is, unfortunately, not resolved in the existing experimental Hb spectra. However, data were reported for human and bovine albumin [21] – a protein found in blood serum. Albumin is similar to hemoglobin in its mass and optical properties at wavelengths away from the characteristic Hb absorption band at 420 nm. The absorption maximum for human albumin is reported as $\varepsilon(187 \text{ nm}) = 86.0 \text{ L g}^{-1} \text{ cm}^{-1}$, corresponding to a value of $\alpha(187 \text{ nm}) = 2.95 \times 10^{-4} \text{ L g}^{-1}$, which is more than four times as high as the peak around 420 nm (Fig. 1).

We model this generic protein absorption using an antisymmetrized Lorentzian curve

$$\alpha_L(\lambda) = a_L \frac{1}{\pi} \frac{\Gamma}{(\lambda - L)^2 + \Gamma^2} - a_L \frac{1}{\pi} \frac{\Gamma}{(\lambda + L)^2 + \Gamma^2}, \quad (14)$$

where $\Gamma = 11.6$ nm is the half width at half maximum of the curve and $L = 187$ nm is the position of its maximum. This model curve fulfills $\alpha_L(-\lambda) = -\alpha_L(\lambda)$. This is important, as the symmetries $\kappa(-\lambda) = -\kappa(\lambda)$ and $n(-\lambda) = n(\lambda)$ are implied when using the KK relations in the form Eq. (10), Eq. (11) or the analogous expressions for the frequency, where they are written as an semi-infinite integral, denoted by the symbol f_0^∞ .

As mentioned before, the deep UV spectrum and hence the exact shape of the peptide absorption line is not available in the literature. For proteins, Woods and O'Bar report that "the increase in absorbance at 187 nm is threefold over that at 205 nm and fourfold over that at 210 nm"[21]. This description fits well to the half width of the curve of $\Gamma = 11.6$ nm. Going to even

lower wavelengths $\lambda \ll 187$ nm there will be more absorption features, since the inner electron shells of the atoms will be excited. We thus expect a variety of overlapping absorption lines at these short wavelengths. On the other hand, this spectral region is fairly far away from the region of interest and the KK relations contain a damping factor of $1/(\lambda^2 - \Lambda^2)$. Hence, the exact line-shapes are practically irrelevant. For our model, it suffices to add to the spectrum a delta-peak of unknown amplitude located at zero wavelength, which accounts for the influence of extreme UV absorption by a constant offset in the real RI: $\alpha_\delta(\lambda) = \lim_{\lambda_\delta \rightarrow 0^+} \frac{\pi}{2} a_\delta \lambda_\delta \delta(\lambda - \lambda_\delta)$.

In this respect, our approach is not different from [9, 10]: We cannot predict the absolute value of the RI of Hb, but we need to determine a constant by comparing to experimental data. However, we apply non-local fitting to optimize this constant, instead of using just one single data point. Thus, our method is more robust to uncertainties in both the absorption spectra and the measured real RIs.

C. Fitting to Literature Values

With this model for the UV absorption, we have an absorption spectrum

$$\alpha(\lambda) = \alpha_{\text{lit}}(\lambda) + \alpha_L(\lambda) + \alpha_\delta(\lambda), \quad (15)$$

where $\alpha_{\text{lit}}(\lambda)$ represents the experimental literature data. For the integral transform \mathcal{K} (cf. Eq. (10)) the contribution from the δ -peak $\alpha_\delta(\lambda)$ is $G_\delta(\lambda) = a_\delta$ and hence constant and the contribution $G_L(\lambda) = a_L \tilde{G}_L(\lambda)$ from the Lorentzian, integrated only over the deep UV part of the spectrum, can be obtained analytically (see appendix B). Here $\tilde{G}_L(\lambda)$ is the contribution for a Lorentzian of unit amplitude. Thus, we are left with

$$G(\lambda) = G_{\text{lit}}(\lambda) + a_L \tilde{G}_L(\lambda) + a_\delta, \quad (16)$$

where only the first term $G_{\text{lit}}(\lambda) := \mathcal{K}[\alpha_{\text{lit}}](\lambda)$ needs to be evaluated numerically.

Numerical evaluation is straightforward. We use an integration scheme, which evaluates the KK relations as a Riemann sum with Taylor expansion at the singularities of the integrand as described, e. g., in [22] and in appendix A. The experimental literature data $\alpha_{\text{lit}}(\lambda)$ comprises two datasets: (1) the absorbance data in the range 228 nm–250 nm [14], which we refer to as "ultraviolet" (UV) and (2) the data in the range 250 nm–1100 nm [8], referred to here as "visible" (VIS). Although our use of the terms "visible" and "ultraviolet" deviates from the usual definition, it is convenient to distinguish between the two datasets:

$$\alpha_{\text{lit}}(\lambda) = \begin{cases} \alpha_{\text{UV}}(\lambda) = \text{data from [14]} & \lambda \in [228, 250] \text{ nm}, \\ \alpha_{\text{VIS}}(\lambda) = \text{data from [8]} & \lambda \in [250, 1100] \text{ nm}, \\ 0 & \text{else.} \end{cases} \quad (17)$$

The numerical KK transform is applied to both parts separately, such that $G_{\text{lit}}(\lambda) = G_{\text{UV}}(\lambda) + G_{\text{VIS}}(\lambda)$.

C.1. Fitting of Free Parameters

Neither of the two free parameters of the model, a_L and a_δ can be computed from literature data a priori with satisfying accuracy. For the peptide absorption a_L , the order of magnitude can be estimated from the semi-quantitative data [21], where the absorbance maximum is given. It is important to keep in mind that the KK transform of the peptide-peak in the deep UV depends much stronger on the center position and the area under the peak than on its actual maximum. Since the peak shape

is not quantitatively known, the peak height does not contain enough information to determine a_L .

The real RI

$$n(\lambda; a_L, a_\delta) = n_{\text{H}_2\text{O}}(\lambda) + c_{\text{Hb}} B(\lambda; a_L, a_\delta) \quad (18)$$

and the real refractive increment

$$B(\lambda; a_L, a_\delta) = G_{\text{lit}}(\lambda) - \underbrace{\frac{n_{\text{H}_2\text{O}}(\lambda) - 1}{\rho_{\text{Hb}}}}_{=: G_{\text{H}_2\text{O}}(\lambda)} + a_L \tilde{G}_L(\lambda) + a_\delta \quad (19)$$

linearly depend on the parameters a_L and a_δ . Thus we use a linear least squares approach to optimize the parameter values.

The empirical model function in [11] is formally identical to ours, but the quantity $\beta(\lambda) = B(\lambda)/n_{\text{H}_2\text{O}}(\lambda)$ was considered instead of $B(\lambda)$, cf. Eq. (9) and Eq. (13). The measurements are given at wavelengths λ_i , $i = 1, \dots, N$ and we denote these experimental values by $\beta^*(\lambda_i)$. We convert them to $B_i^* = \beta^*(\lambda_i) n_{\text{H}_2\text{O}}(\lambda_i)$. In the following, the B_i^* will be referred to simply as “the measurement data”.

At each wavelength, the increment $B_i := B(\lambda_i)$ consists of a fixed part resulting from numerical KK transformation

$$B_{0,i} = G_{\text{lit}}(\lambda_i) + G_{\text{H}_2\text{O}}(\lambda_i) \quad (20)$$

and a function yet to be determined, which models the deep UV contributions

$$f_i = a_L \tilde{G}(\lambda_i) + a_\delta \stackrel{\text{def. } h_r(\lambda)}{=} \sum_{r=L,\delta} a_r h_r(\lambda_i). \quad (21)$$

Switching to matrix-vector notation, we write this function vector as $\mathbf{f} = \mathbf{H} \mathbf{a}$, with $\mathbf{H} := \{h_r(\lambda_i)\}_{ir} \in \mathbb{R}^{N \times 2}$ and $\mathbf{a} = (a_L, a_\delta)^T$ is the parameter vector.

Now we want to minimize the deviation between KK results with deep UV absorbance model \mathbf{B} and measurement data \mathbf{B}^*

$$\mathbf{B}^* - \mathbf{B} = \mathbf{y} - \mathbf{f}, \quad (22)$$

where $\mathbf{y} = \mathbf{B}^* - \mathbf{B}_0$ is the data vector. The entries of vector \mathbf{B}_0 are given in Eq. (20). The linear least squares problem is then $\chi^2(\mathbf{a}) \rightarrow \min$ with

$$\begin{aligned} \chi^2(\mathbf{a}) &:= (\mathbf{y} - \mathbf{f})^T \mathbf{W} (\mathbf{y} - \mathbf{f}) \\ &= \sum_{\lambda_i=250 \text{ nm}}^{1100 \text{ nm}} w_{ij} [B^*(\lambda_i) - B(\lambda_i; \mathbf{a})] [B^*(\lambda_j) - B(\lambda_j; \mathbf{a})], \end{aligned} \quad (23)$$

where $\mathbf{W} = \{w_{ij}\}_{i,j=1}^N$ is a weight matrix given by the inverse of the covariance matrix \mathbf{V} of the data vector. The conditions for minimal $\chi^2(\mathbf{a})$ are solved by standard linear algebra, which yields

$$\hat{\mathbf{a}} = \arg \min \chi^2(\mathbf{a}) = (\mathbf{H}^T \mathbf{V}^{-1} \mathbf{H})^{-1} \mathbf{H}^T \mathbf{V}^{-1} \mathbf{y} \quad (24)$$

$$\hat{\mathbf{f}} = \mathbf{H} \hat{\mathbf{a}} = \underbrace{\mathbf{H} (\mathbf{H}^T \mathbf{V}^{-1} \mathbf{H})^{-1} \mathbf{H}^T \mathbf{V}^{-1}}_{=: \mathbf{F}} \mathbf{y} \quad (25)$$

for parameter and function vector and $\hat{\mathbf{B}} = \mathbf{B}_0 + \hat{\mathbf{f}}$ for the refractive increment. The resulting amplitude of the Lorentzian is shown in Fig. 1 as generic peptide absorbance.

C.2. Deoxyhemoglobin

Both, the absorption spectra of oxygenated and deoxygenated hemoglobin are well known, cf. Fig. 1. However, the method of [8] to measure the real RI could only be applied to oxyhemoglobin, whereas measurements with deoxyhemoglobin were not possible due to precipitation resulting in backscattering of light from highly concentrated solutions of deoxyhemoglobin. Nevertheless, the KK analysis allows to derive a result for the real refractive increment of deoxyhemoglobin. To this end, we use the same model for the deep UV absorbance as above, Lorentzian and delta-peak, with the coefficients $\hat{a}_L, \hat{a}_\delta$ found by the least-squares fit for oxyhemoglobin. Combining this with the KK transform of the spectrum $\alpha^{\text{deoxy}}(\lambda)$ for deoxyhemoglobin, we calculate the real refractive increment according to

$$\begin{aligned} B^{\text{deoxy}}(\lambda_i) &= B_0^{\text{deoxy}}(\lambda_i) + \hat{f}(\lambda_i) \\ &= G_{\text{lit}}^{\text{deoxy}}(\lambda_i) + G_{\text{H}_2\text{O}}(\lambda_i) + \hat{f}(\lambda_i). \end{aligned} \quad (26)$$

The reason to simply use the same deep UV model curve for oxyhemoglobin as well as for deoxyhemoglobin is that oxygenation affects the heme-groups in the hemoglobin complex. The absorption peaks at about 420 nm and 560 nm are altered by oxygenation (cf. Fig. 1) but not the peptide backbone causing the deep UV absorption.

D. Uncertainties

Both, the Kramers-Kronig transformation and the linear least-squares fit to the data are linear transformations, which can formally be carried out by matrix multiplication. Hence, it is easy to perform the uncertainty propagation in terms of mean values and covariance matrices. A detailed description is given in appendix C. All values for uncertainties given here correspond to one standard deviation.

An important uncertainty contribution stems from the uncertainty of the hemoglobin concentration c_{Hb} . Because this influences the concentration-specific transmittance and reflectance spectra by a global factor, the uncertainties of the resulting real refractive increment are strongly correlated between all wavelengths, i. e., the correlation coefficient

$$r_{ij} := \frac{\text{cov}(B_i, B_j)}{\sqrt{\text{var}(B_i) \text{var}(B_j)}} \quad (27)$$

is close to +1 even if $\lambda_i - \lambda_j$ is large. Here “cov” and “var” denote covariance and variance, respectively. In such a case the use of the diagonal elements of the covariance matrix only, i. e., the variances, may lead to unnecessarily less significant results with respect to the uncertainty estimation. When, for instance, the difference between two random variables X, Y is considered, the variance is

$$\text{var}(X - Y) = \text{var}(X) + \text{var}(Y) - 2 \text{cov}(X, Y), \quad (28)$$

which may be small even if $\text{var}(X), \text{var}(Y)$ are large.

3. RESULTS AND DISCUSSION

A. Real Part of Refractive Index for Oxy- and Deoxyhemoglobin

Fig. 2 shows the result of the presented KK analysis for the real refractive increment $\hat{B}(\lambda)$ for oxyhemoglobin along with the experimental data $B^*(\lambda)$ from [11]. The uncertainties are

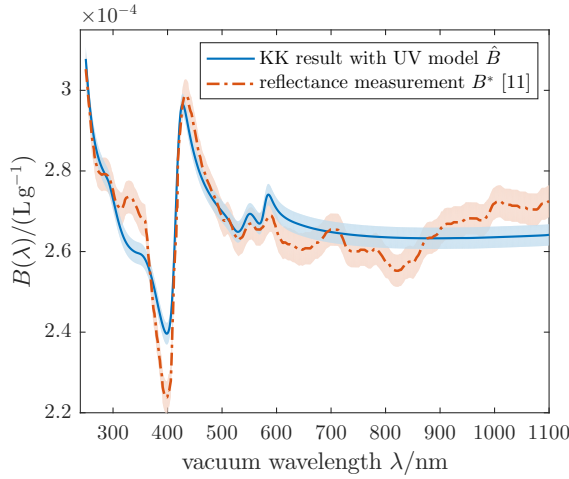


Fig. 2. Real refractive increment $B(\lambda)$ of aqueous solutions of oxyhemoglobin: Experimental data [11] and results from this work fitted to the data. The shaded bands indicate the measurement uncertainties given in [11] and computed in appendix C, respectively.

shown as shaded bands, where the half-width of the band corresponds to one standard deviation derived by covariance-matrix calculus. The analogue result for deoxygenated hemoglobin is shown in Fig. 3. Fig. 4 shows the derivative $\hat{B}'(\lambda) = d\hat{B}(\lambda)/d\lambda$. Here the strong correlation is eliminated, resulting in much smaller uncertainties. It is evident from Fig. 4 that the main uncertainty of the result concerns the exact vertical position of the curve $\hat{B}(\lambda)$, whereas the uncertainties related to its shape, described equivalently by the derivative $\hat{B}'(\lambda)$, are smaller.

The result $\hat{B}(\lambda)$ of the KK analysis for oxyhemoglobin and the experimental data $B^*(\lambda)$ as shown in Fig. 2 have a similar overall shape, but there are deviations which cannot be accounted for by the measurement uncertainties of $B^*(\lambda)$ given in [11] and the uncertainties of the KK result derived as described in appendix C. For instance, the difference between the peak at 433 nm and the dip at 399 nm for B^* is

$$B^*(433 \text{ nm}) - B^*(399 \text{ nm}) = (7.5 \pm 0.6) \times 10^{-5} \text{ L g}^{-1}$$

while that for our result is

$$\hat{B}(433 \text{ nm}) - \hat{B}(399 \text{ nm}) = (5.47 \pm 0.06) \times 10^{-5} \text{ L g}^{-1}.$$

The small value for the uncertainty of $\hat{B}(433 \text{ nm}) - \hat{B}(399 \text{ nm})$ is due to the fact that the strongly correlated concentration contributions to the uncertainty cancel out almost completely for this difference. This observation also holds for the derivative $\hat{B}'(\lambda)$ (cf. Fig. 4). The difference between the two values clearly exceeds the uncertainties.

The deviations between $\hat{B}(\lambda)$ and $B^*(\lambda)$ can not be attributed to unknown spectral absorptions outside the 250 nm–1100 nm range, since features producing such discrepancies would necessarily be inside this wavelength range. We have modeled important spectral absorptions at the UV end of the spectrum. Concerning possible IR absorptions that are not considered in the proposed model, we give the following notes: The absorption spectra of aqueous hemoglobin solutions in the IR between 1.1 μm and 2.6 μm are dominated by water [8] indicating that the imaginary refractive increment of Hb is very low in this region. Hypothetical absorption lines due to Hb at

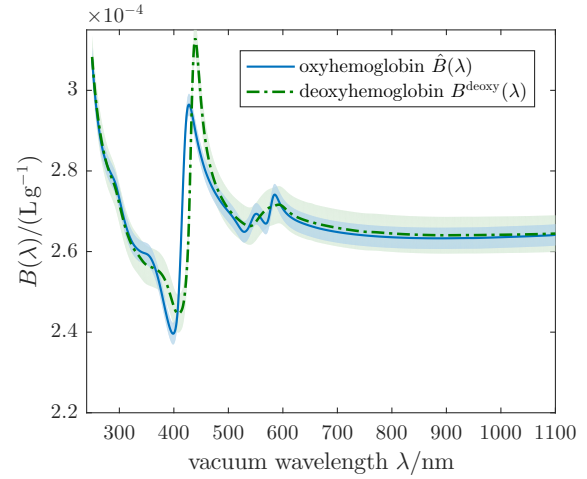


Fig. 3. Real refractive increment of aqueous hemoglobin solutions: Result for deoxyhemoglobin obtained by KK relations with the same model for deep UV absorbance as for oxyhemoglobin. Cf. Fig. 2. Estimated standard deviations (shaded bands) are larger for deoxyhemoglobin because $B^{\text{deoxy}}(\lambda)$ is composed of more terms with uncorrelated concentration uncertainties than $\hat{B}(\lambda)$.

even longer wavelengths would contribute to the real refractive index increment $B(\lambda)$ in the form of constants or functions with a gentle negative slope. Any possible influence of the long-wavelength end of the spectrum of Hb would thus change the agreement between our result $\hat{B}(\lambda)$ and the literature data $B^*(\lambda)$ for the worse. Thus we conclude that no important contribution to the absorption spectrum was missed at the long-wavelength end. The KK relations themselves are valid as long as the framework within which the data were measured holds, i. e., classical electrodynamics and linear, causal media. Optical activity of Hb has been examined previously [14, 23] and can be ruled out as well, since the expected effect is too weak. Furthermore, we can exclude biological variability, since absorption and reflectance/refraction data were measured on the same type of sample [8, 11]. This implies that the absorption and refraction data presented in [8, 11] are not self-consistent with the given measurement uncertainties.

Lastly, we address the question, whether these discrepancies are of practical importance. At $\lambda = 399 \text{ nm}$, where the discrepancy is largest, one has $B^* = 2.24 \times 10^{-4} \text{ L g}^{-1}$ from [11] and $\hat{B} = 2.41 \times 10^{-4} \text{ L g}^{-1}$ for our analysis. At a concentration of $c_{\text{Hb}} = 340 \text{ g L}^{-1}$ the resulting real RIs are $n^* = n_{\text{H}_2\text{O}} + c_{\text{Hb}} B^* = 1.420$ and $\hat{n} = n_{\text{H}_2\text{O}} + c_{\text{Hb}} \hat{B} = 1.426$, respectively and the residual is $|\hat{n} - n^*| = 0.006 = 0.4\% n^*$. Since this value is in the sub-percent region it may, at first glance, seem unimportant whether one uses n^* or \hat{n} . However, when RBCs are examined with optical methods such as phase contrast microscopy or light scattering in a flow cytometer, they are usually immersed in water with an RI of $n_{\text{H}_2\text{O}}(399 \text{ nm}) = 1.344$, or a saline solution of slightly higher RI. Hence the complex contrast between cell and surrounding medium is

$$m - 1 := \frac{n}{n_{\text{H}_2\text{O}}} - 1 = \begin{cases} 0.061 + 0.008i & \text{[11]} \\ 0.057 + 0.008i & \text{our result} \end{cases}. \quad (29)$$

In phase contrast microscopy, the signal for the optical thickness of the cell is directly proportional to the contrast $m - 1$. It

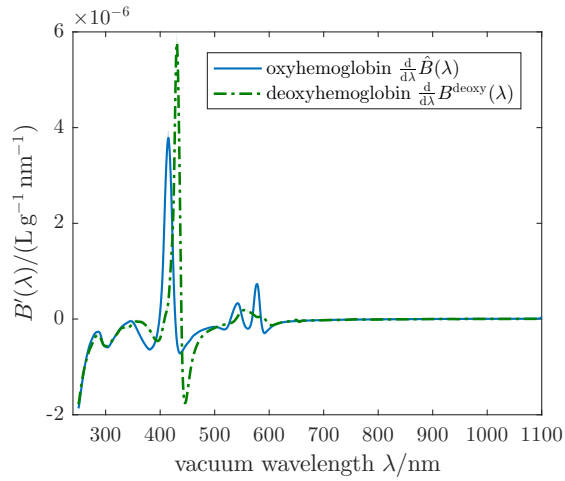


Fig. 4. Derivative of the real refractive increment $B'(\lambda) = \frac{d}{d\lambda}B(\lambda)$: Comparison between results for deoxyhemoglobin and oxyhemoglobin. Estimated standard deviations (shaded bands, barely visible) of $B'(\lambda)$ are much smaller than for $B(\lambda)$ (Fig. 3). This is because most of the (strongly correlated) concentration uncertainty cancels out in the derivative.

is also a parameter governing the light scattering by cells. The Rayleigh-Gans-Debye theory is an approximate description of light scattering for the limiting case of particles with low contrast and moderate size. It predicts a scattered electric field proportional to $m - 1$. The real parts of the above two values for $m - 1$ differ by more than 7%, indicating that any quantitative analysis of the interaction of RBCs with light that requires a priori knowledge of the contrast can not be more accurate than this.

B. Comparison to Previous KK Analyses

We will now briefly review the previous investigations employing KK relations [9, 10] and compare the methods. In [9], the authors started from Eq. (10) and applied it to the Hb absorption spectra in a finite spectral range, i. e., instead of Eq. (6) they assumed

$$\kappa_{[9]}(\lambda) = c_{\text{Hb}} \alpha_{\text{VIS}}(\lambda) = c_{\text{Hb}} \begin{cases} \alpha(\lambda) & \lambda \in [a, b] \\ 0 & \text{else} \end{cases}, \quad (30)$$

where $[a, b]$ is the measured spectral range, i. e., here $[a, b] = [250, 1100]$ nm. The authors then used a subtractive form of the KK relations, where the difference $n(\lambda) - n(\lambda_0)$ is considered which yields

$$n_{[9]}(\lambda) = n(\lambda_0) + c_{\text{Hb}} [G_{\text{VIS}}(\lambda) - G_{\text{VIS}}(\lambda_0)]. \quad (31)$$

Here, $G_{\text{VIS}}(\lambda) := \mathcal{K}[\alpha_{\text{VIS}}](\lambda)$ is the dispersion resulting from the measured spectrum. The free parameter $n(\lambda_0)$ is fixed by a refractometric measurement at wavelength $\lambda_0 = 800$ nm. If the non-subtractive KK relations had been used instead, the result would have been

$$n(\lambda) = 1 + c_{\text{Hb}} G_{\text{VIS}}(\lambda), \quad (32)$$

which is off the true value by a significant amount. One can remove this discrepancy by replacing the 1 in the above expression by a free parameter, which can be interpreted as deep UV absorption. Again, this free parameter can be fixed by a single

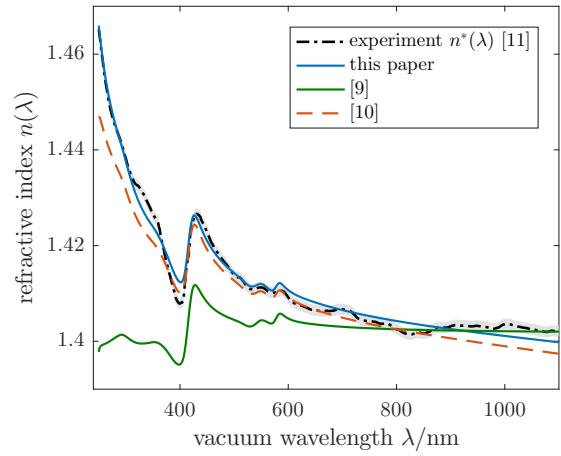


Fig. 5. Comparison between the experimental real RI derived from measured refractive increment of Hb solutions [11] and the water RI [19] (measurement uncertainty indicated by shaded band) and different Kramers-Kronig analyses. Concentration is $c_{\text{Hb}} = 287 \text{ g L}^{-1}$. The method in [9] ignores absorption outside the measured range and in [10] the UV and IR absorption of water was taken into account. In the present work the excluded water fraction was accounted for, as well as a model for deep UV absorbance. All KK methods were applied to the same dataset depicted in Fig. 1. Curves calculated according to [9, 10] are matched to the experimental curve at $\lambda_0 = 800$ nm. The two free parameters characterizing the deep UV model in our method are determined by a global fit to the experimental refractive increment.

measurement at λ_0 . The result is then the same as in Eq. (31). However, the subtractive KK transform $\mathcal{K}[\alpha](\lambda) - \mathcal{K}[\alpha](\lambda_0)$ can be re-written into a single integral where the kernel decays faster than in the standard KK relations, which is numerically favorable and thus given as an argument for the use of subtractive relations. Thus, the subtractive form of KK relations masks the lack of knowledge of the absorption spectrum outside the measured spectral range: At least one important absorption peak at short wavelengths has apparently been omitted. As long as the missing peak is far away from the region of interest, the simple addition of a constant works fine. However, if the location of the peak becomes important as is the case for water, this model is insufficient.

In [10], the authors made the ansatz

$$\kappa_{[10]}(\lambda) = \kappa_{\text{H}_2\text{O}}(\lambda) + c_{\text{Hb}} \alpha_{\text{VIS}}(\lambda). \quad (33)$$

for the imaginary RI of the Hb solution, which takes the absorption due to water into account but neglects the excluded volume effect for water in contrast to our approach in Eq. (6). Apart from this difference, the formal application of the KK relations in the present work is identical to that in [10]. The result was

$$n_{[10]}(\lambda) = n_{\text{H}_2\text{O}}(\lambda) + c_{\text{Hb}} G_{\text{VIS}}(\lambda), \quad (34)$$

which provides also a theoretical derivation of the empirical finding $n(\lambda) = n_{\text{H}_2\text{O}}(\lambda)[1 + c_{\text{Hb}} \beta(\lambda)]$ reported in [11]. However, the result that $\beta(\lambda) = G_{\text{VIS}}(\lambda)/n_{\text{H}_2\text{O}}(\lambda)$ is incomplete, as we have discussed. Subtractive KK relations were used as well to match the RI at $\lambda_0 = 800$ nm.

To compare these two previously presented methods with ours, we applied them to the spectra of oxyhemoglobin pre-

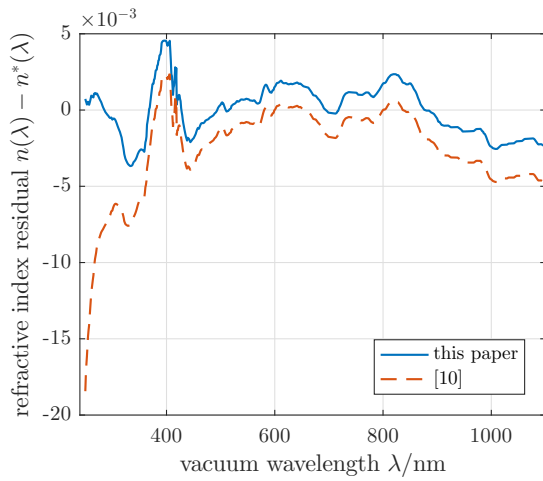


Fig. 6. Residuals between calculated real RI $n(\lambda)$ and experimental real RI $n^*(\lambda)$ [11] for our method and the method applied in [10], cf. Fig. 5.

sented in [8] and shown in Fig. 1. As an example, a concentration of $c_{\text{Hb}} = 287 \text{ g L}^{-1}$ was assumed and $n(\lambda_0 = 800 \text{ nm}) = 1.403$ was taken from [8] as well. The comparison of the two methods applied in [9, 10] with our method and the experimental dispersion curve given in [11] is shown in Fig. 5. Neglecting the water influence as in [9] yields a dispersion curve which substantially deviates from the measurement (dash-dotted black line in Fig. 5) everywhere, except at and above λ_0 , where it was matched. With the water absorption and the resulting dispersion taken into account [10] the agreement with the experimental result is already much better. However, the result from [10] and experimental curve substantially differ in the UV below 375 nm. The agreement in the UV is much better in our approach. This is also evident from Fig. 6, where the residuals between KK computations and experiment are plotted.

4. SUMMARY

The complex refractive index of a hemoglobin solution, which forms the cytoplasm of erythrocytes and determines their optical properties can be computed as

$$n(\lambda) = n_{\text{H}_2\text{O}}(\lambda) + i\kappa_{\text{H}_2\text{O}}(\lambda) + c_{\text{Hb}}[B(\lambda) + i\alpha(\lambda)], \quad (35)$$

where $\kappa_{\text{H}_2\text{O}}(\lambda)$ is negligibly small for $\lambda \in [250, 1100]$ nm and physiological hemoglobin concentrations c_{Hb} . In the present work, we have computed the real refractive increment $B(\lambda)$ from experimental spectra of the imaginary refractive increment $\alpha(\lambda)$ for $\lambda \in [250, 1100]$ nm. We formally separated the solution's imaginary RI into a water and a hemoglobin part and then applied the Kramers-Kronig relations to obtain the real RI and thus an expression for $B(\lambda)$, Eq. (13). The absorption spectra available in the literature [8, 14] do not resolve the strong UV absorbance of hemoglobin's peptide-backbone. Hence we modeled it by a Lorentzian line of unknown amplitude, which introduces a free parameter a_L into the expression for $B(\lambda)$. A second free parameter a_δ is introduced as a wavelength-independent term accounting for extreme UV absorbance, cf. Eq. (19). These two free parameters were determined by a linear least squares fit to the literature data $B^*(\lambda)$ [11], the result of the fit is denoted by $\hat{B}(\lambda)$.

We evaluated spectra for oxygenated and deoxygenated hemoglobin. Data files of the results are provided as supplementary material for $\hat{B}(\lambda)$ (Data File 1), $B^{\text{deoxy}}(\lambda)$ (Data File 3), the corresponding covariance matrices (Data Files 2 and 4), the converted literature data for $\alpha(\lambda)$ and $\alpha^{\text{deoxy}}(\lambda)$ [8] and the values for $n_{\text{H}_2\text{O}}(\lambda)$ computed according to [19] (Data Files 1 and 3) as well as for $\hat{B}'(\lambda)$ (Data File 5).

The uncertainties for the curve $\hat{B}(\lambda)$ were computed and reveal that its shape is resolved much more accurately than in the measurements $B^*(\lambda)$ in [11]. The analysis furthermore shows that the real refractive increments for oxygenated and deoxygenated hemoglobin differ significantly from each other for wavelengths between 350 nm and 600 nm. In the vicinity of the absorption band at 420 nm, deviations between our result for the real refractive increment and the experimental values [11] clearly exceed the measurement uncertainties, where the curve obtained by our KK analysis has a much smoother shape and does not exhibit the non-monotonic up-and-down movements for wavelengths larger than 600 nm of the data presented in [11].

A. APPENDIX: NUMERICAL INTEGRATION SCHEME FOR KRAMERS-KRONIG RELATIONS

For numerical integration of KK relations, we follow the concept described in [22]: a Riemann sum with Taylor expansion at the singularities of the integrand. Numerical stability was tested by comparing to the analytical transformations of different Lorentzian and rectangular profiles.

We want to evaluate numerically the expression

$$\begin{aligned} \pi G(\lambda) &= -2 \int_{\lambda_a}^{\lambda_b} \frac{\lambda}{\Lambda} \frac{\lambda}{\Lambda^2 - \lambda^2} \alpha(\Lambda) d\Lambda \\ &= \int_{\lambda_a}^{\lambda_b} \left(\frac{2}{\Lambda} - \frac{1}{\Lambda + \lambda} - \frac{1}{\Lambda - \lambda} \right) \alpha(\Lambda) d\Lambda. \end{aligned} \quad (36)$$

The measurement data are given at discrete points

$$\alpha_i := \alpha(\lambda_i), \quad (37)$$

$$\lambda_i := \lambda_a + t \left(i - \frac{1}{2} \right), \quad i = 1, \dots, N, \quad (38)$$

where $\lambda_1 = 250$ nm, $\lambda_N = 1100$ nm and $t = 1$ nm. Hence $\lambda_a = 249.5$ nm, $\lambda_b = 1100.5$ nm and $N = 851$. We only evaluate the integral at the grid points $G_i := G(\lambda_i)$. The third term in the integral has a singularity at $\lambda = \Lambda$. The first two terms are not singular, hence no principal value integrals have to be used here. All integrals for non-singular integrands are approximated by Riemann sums, including the third term for $\Lambda \notin [\lambda_i - t/2, \lambda_i + t/2]$. The remaining principal value integral can be re-written by Taylor series expansion of the integrand. Using only the lowest non-vanishing order yields

$$\pi G_i \approx \sum_{j=1}^N \left(\frac{2}{\lambda_j} - \frac{1}{\lambda_j + \lambda_i} \right) \alpha_j t - \sum_{\substack{j=1 \\ j \neq i}}^N \frac{1}{\lambda_j - \lambda_i} \alpha_j t - t \alpha'_i. \quad (39)$$

Numerically, we use the nearest-neighbor lattice-derivatives

$$t \alpha'_i = \begin{cases} (\alpha_{i+1} - \alpha_{i-1})/2 & 1 < i < N \\ \alpha_2 - \alpha_1 & i = 1 \\ \alpha_N - \alpha_{N-1} & i = N \end{cases}. \quad (40)$$

Note that Eq. (39) can also be written as $G = K\alpha$, where K is a $N \times N$ matrix.

B. APPENDIX: UV DOMAIN KRAMERS-KRONIG-TRANSFORM OF LORENTZIAN CURVE

If the KK transform (Eq. (10)) is applied to the antisymmetric Lorentzian line in the wavelength domain Eq. (14) the result is

$$\begin{aligned} \mathcal{K}[\alpha_L](\lambda) = & a_L \frac{1}{\pi} \left(\frac{\lambda - L}{(\lambda - L)^2 + \Gamma^2} + \frac{L}{L^2 + \Gamma^2} \right) \\ & - a_L \frac{1}{\pi} \left(\frac{\lambda + L}{(\lambda + L)^2 + \Gamma^2} - \frac{L}{L^2 + \Gamma^2} \right). \end{aligned} \quad (41)$$

In our work, however, we need to integrate only over the deep ultraviolet spectrum below a threshold λ_a . The analytical expression for this reads

$$\begin{aligned} G_L(\lambda) = & \frac{1}{\pi} \int_{-\lambda_a}^{\lambda_a} \left(\frac{1}{\Lambda} - \frac{1}{\Lambda - \lambda} \right) \alpha_L(\Lambda) d\Lambda \\ = & \frac{a_L}{\pi^2} \left\{ \frac{1}{2} \ln \left(\frac{(\lambda_a - L)^2 + \Gamma^2}{(\lambda_a + L)^2 + \Gamma^2} \right) \right. \\ & \times \left[\frac{\Gamma}{(\lambda - L)^2 + \Gamma^2} + \frac{\Gamma}{(\lambda + L)^2 + \Gamma^2} - \frac{2\Gamma}{L^2 + \Gamma^2} \right] \\ & - \ln \left(\left| \frac{\lambda_a - \lambda}{\lambda_a + \lambda} \right| \right) \times \left[\frac{\Gamma}{(\lambda - L)^2 + \Gamma^2} - \frac{\Gamma}{(\lambda + L)^2 + \Gamma^2} \right] \\ & + \left(\pi - \arctan \frac{\Gamma}{\lambda_a - L} - \arctan \frac{\Gamma}{\lambda_a + L} \right) \\ & \left. \times \left[\frac{\lambda - L}{(\lambda - L)^2 + \Gamma^2} - \frac{\lambda + L}{(\lambda + L)^2 + \Gamma^2} + \frac{2L}{L^2 + \Gamma^2} \right] \right\} \end{aligned} \quad (42)$$

for $\lambda > \lambda_a$. Eq. (42) is useful to describe the deep UV part of the absorption spectrum without the need for numerical integration.

We also define the transformation for unit amplitude $\tilde{G}_L(\lambda)$, such that $G_L(\lambda) = a_L \tilde{G}_L(\lambda)$.

C. APPENDIX: DETAILS OF UNCERTAINTY PROPAGATION

A. Uncertainties of Input Data

We now recapitulate how spectral data are measured, in order to understand which contributions to the combined uncertainties occur in the problem at hand.

The absorption spectra (inverse absorption length $\mu_a(\lambda)$, imaginary RI $\kappa(\lambda)$) are measured via the attenuation of a beam of light passing through a sample of known thickness. This is performed for a number of wavelengths λ_i , $i = 1, \dots, N$. The molar extinction coefficient $\varepsilon_M(\lambda)$ and the imaginary refractive increment $\alpha(\lambda)$ are obtained from these quantities by dividing with the separately determined molar/mass concentration of Hb in the solution.

In [8, 11] spectral reflectance measurements were performed and evaluated using the Fresnel equation Eq. (8) to obtain the real RI $n(\lambda)$. To determine the experimental value of the real refractive increment $B^*(\lambda)$, several curves at different concentrations c_{Hb} were recorded and the slope of $n(\lambda)$ with respect to c_{Hb} was computed for all λ and normalized to the known water RI to obtain $\beta^*(\lambda)$.

Having this in mind, measurement uncertainties of the following quantities need to be taken into account:

1. Detector/instrument noise in the absorption spectra. This affects the inverse absorption length $\mu_a(\lambda)$ in [8] and the molar extinction coefficient $\varepsilon_M(\lambda)$ in [14].

2. Detector/instrument noise in the reflectance spectra [8, 11], resulting in a wavelength-independent uncertainty of $3 \times 10^{-6} \text{ L g}^{-1}$ [11] for the real refractive increment $\beta^*(\lambda)$.
3. Uncertainties of the solutions' Hb concentration c_{Hb} .
4. Uncertainty of the hemoglobin density ρ_{Hb} relating mass concentration c_{Hb} and volume fraction ϕ . Here we assume one digit, i. e., $u_{\rho_{\text{Hb}}} = 10 \text{ g L}^{-1} = 0.75\% \rho_{\text{Hb}}$.
5. Uncertainty of the complex RI of water. This influence is negligible.

These uncertainties can be divided into two classes, separating 1.–2. from 3.–4.:

- (i) Noise in the measured reflectance and transmittance spectra, affecting the spectral data locally. The corresponding quantities are labeled with the subscript "noise". As a model, we assume white noise, i. e., two measurement errors at different wavelengths are not correlated.
- (ii) Measurement uncertainties in scalar quantities ($c_{\text{Hb}}, \rho_{\text{Hb}}$) occurring as prefactors in the spectra. These affect the spectra by a global factor, i. e., the errors at different wavelengths have correlation coefficient +1. The corresponding quantities are labeled with a subscript "conc".

In addition there are model errors, which arise due to unknown absorption spectra outside the measured range and which we discuss in appendix E.

B. Error Model and Uncertainty Propagation

For any random vector $\xi \in \mathbb{R}^N$ and any non-random linear transform $A \in \mathbb{R}^{N \times N}$, we have for $\eta = A\xi$

$$\mathbb{E}(\eta) = A \mathbb{E}(\xi) \quad (43)$$

$$\mathbb{V}(\eta) = A \mathbb{V}(\xi) A^T, \quad (44)$$

where \mathbb{E} denotes the expectation value (or mean) and

$$[\mathbb{V}(\xi)]_{ij} = \text{cov}(\xi_i, \xi_j) = \mathbb{E} \left([\xi_i - \mathbb{E}(\xi_i)] [\xi_j - \mathbb{E}(\xi_j)] \right) \quad (45)$$

denotes the covariance matrix. This is independent of the underlying probability distribution, only implying that the first and second moments exist. We restrict our uncertainty analysis to mean values and covariance matrix, which describes the corresponding probability distributions fully only in the special case of a normal distribution.

The uncertainties of the literature absorption spectra are not given; neither the noise nor the concentration uncertainties are quantified. We thus estimate and model them as follows. The covariance matrix for the absorption spectra is assumed to be $\mathbb{V}(\alpha) = \mathbb{V}_{\text{noise}}(\alpha) + \mathbb{V}_{\text{conc}}(\alpha)$. Here

$$\mathbb{V}_{\text{noise}}(\alpha) = \sigma_{\text{noise,rel}}^2 \text{diag}(\alpha)^2 \quad (46)$$

is the local/uncorrelated part due to (white) detector noise. This matrix is diagonal.

$$\mathbb{V}_{\text{conc}}(\alpha) = \sigma_{\text{conc,rel}}^2 \alpha \alpha^T \quad (47)$$

is the global/correlated part due to concentration uncertainty. This matrix has a tensor-product structure. We use $\sigma_{\text{noise,rel}} = 0.5\%$ for the relative noise level and $\sigma_{\text{conc,rel}} = 1\%$ for the relative concentration uncertainty [24].

Eq. (47) is motivated as follows: Concentration errors change a spectrum by a global factor, such that the measured value

$$\boldsymbol{\alpha}_{\text{meas}} = (1 + \zeta)\boldsymbol{\alpha}, \quad (48)$$

is off the (unknown) true value $\boldsymbol{\alpha}$. We assume this error to be unbiased, i. e., $\mathbb{E}(\zeta) = 0$ and $\sqrt{\text{var}(\zeta)} = \sigma_{\text{conc,rel}}$ corresponds to the relative concentration uncertainty of the solution. I. e., $\mathbb{E}(\boldsymbol{\alpha}_{\text{meas}}) = \boldsymbol{\alpha}$, and

$$\begin{aligned} \mathbf{V}(\boldsymbol{\alpha}_{\text{meas}}) &= \text{var}(\zeta) \boldsymbol{\alpha} \boldsymbol{\alpha}^T = \underbrace{\text{var}(\zeta)}_{=\sigma_{\text{conc,rel}}^2} \mathbb{E}(\boldsymbol{\alpha}_{\text{meas}}) \mathbb{E}(\boldsymbol{\alpha}_{\text{meas}})^T \\ &\approx \sigma_{\text{conc,rel}}^2 \boldsymbol{\alpha}_{\text{meas}} \boldsymbol{\alpha}_{\text{meas}}^T, \end{aligned} \quad (49)$$

which is Eq. (47). In the following we will drop the distinction between unknown true values and measured values and substitute the latter for the former.

This error model is formally invariant under linear transformation. The measured value of some quantity obtained by a linear transform \mathbf{A} (e. g., the KK transform)

$$\boldsymbol{\eta}_{\text{meas}} = \mathbf{A} \boldsymbol{\alpha}_{\text{meas}} = (1 + \zeta)\mathbf{A} \boldsymbol{\alpha} = (1 + \zeta) \boldsymbol{\eta}, \quad (50)$$

is formally identical to Eq. (48) such that the variance $\mathbf{V}(\boldsymbol{\eta}_{\text{meas}})$ can be computed from $\mathbb{E}(\boldsymbol{\eta}_{\text{meas}})$ in the same manner as for the original quantity $\boldsymbol{\alpha}$, i. e., $\mathbf{V}(\boldsymbol{\eta}_{\text{meas}}) = \text{var}(\zeta)\boldsymbol{\eta}\boldsymbol{\eta}^T$.

C. Uncertainty Propagation in Kramers-Kronig Relations

For discrete data points, the KK relations can be written in matrix vector form, i. e., $\mathbf{G} = \mathbf{K} \boldsymbol{\alpha}$, where \mathbf{K} is a $N \times N$ matrix (see appendix A). If $\mathbf{V}(\boldsymbol{\alpha})$ is the (co-)variance matrix of the spectrum $\boldsymbol{\alpha}$, then the covariance matrix of the transform \mathbf{G} is

$$\mathbf{V}(\mathbf{G}) = \mathbf{K} \mathbf{V}(\boldsymbol{\alpha}) \mathbf{K}^T \quad (51)$$

and with the model for $\mathbf{V}(\boldsymbol{\alpha})$ one obtains

$$\mathbf{V}(\mathbf{G}) = \mathbf{V}_{\text{noise}}(\mathbf{G}) + \mathbf{V}_{\text{conc}}(\mathbf{G}), \quad (52)$$

where $\mathbf{V}_{\text{conc}}(\mathbf{G}) = \sigma_{\text{conc,rel}}^2 \mathbf{G} \mathbf{G}^T$ has the same tensor product structure as $\mathbf{V}_{\text{conc}}(\boldsymbol{\alpha})$ in Eq. (47). In contrast, $\mathbf{V}_{\text{noise}}(\mathbf{G}) = \mathbf{K} \mathbf{V}_{\text{noise}}(\boldsymbol{\alpha}) \mathbf{K}^T$ is, unlike $\mathbf{V}_{\text{noise}}(\boldsymbol{\alpha})$, not diagonal, because of the non-locality of the KK transform.

D. Uncertainty Propagation in Linear Fit

The covariance matrix $\mathbf{V}(\mathbf{y})$ of

$$\mathbf{y} = \mathbf{B}^* - \mathbf{B}_0 = \mathbf{B}^* - \mathbf{G}_{\text{VIS}} - \mathbf{G}_{\text{UV}} - \mathbf{G}_{\text{H}_2\text{O}} \quad (53)$$

is obtained by

$$\begin{aligned} \mathbf{V}(\mathbf{y}) &= \mathbf{V}(\mathbf{B}^*) + \mathbf{V}(\mathbf{B}_0) \\ &= \mathbf{V}(\mathbf{B}^*) + \mathbf{V}(\mathbf{G}_{\text{VIS}}) + \mathbf{V}(\mathbf{G}_{\text{UV}}) + \mathbf{V}(\mathbf{G}_{\text{H}_2\text{O}}). \end{aligned} \quad (54)$$

This decomposes into a noise and a concentration term $\mathbf{V}(\mathbf{y}) = \mathbf{V}(\mathbf{y})_{\text{noise}} + \mathbf{V}(\mathbf{y})_{\text{conc}}$. For the contributions from concentration uncertainties, one finds (cf. Eq. (54) and Eq. (49))

$$\mathbf{V}_{\text{conc}}(\mathbf{y}) = \sum_{j=1}^4 \mathbf{v}_j \mathbf{v}_j^T. \quad (55)$$

with

$$\begin{aligned} \mathbf{v}_1 &:= \sigma_{\text{conc,rel}} \mathbf{B}^*, & \mathbf{v}_2 &:= \sigma_{\text{conc,rel}} \mathbf{G}_{\text{VIS}}, \\ \mathbf{v}_3 &:= \sigma_{\text{conc,rel}} \mathbf{G}_{\text{UV}}, & \mathbf{v}_4 &:= \frac{u_{\rho_{\text{Hb}}}}{\rho_{\text{Hb}}} \mathbf{G}_{\text{H}_2\text{O}}. \end{aligned} \quad (56)$$

Similarly, we obtain $\mathbf{V}_{\text{conc}}(\mathbf{B}^*) = \mathbf{v}_1 \mathbf{v}_1^T$.

However, for weighting the linear fit, we do not use this covariance matrix, but only the noise terms, i. e., $\mathbf{V} = \mathbf{V}_{\text{noise}}(\mathbf{y})$ with

$$\mathbf{V}_{\text{noise}}(\mathbf{y}) = \mathbf{V}_{\text{noise}}(\mathbf{B}^*) + \mathbf{K} \mathbf{V}_{\text{noise}}(\boldsymbol{\alpha}_{\text{VIS}}) \mathbf{K}^T + \mathbf{K} \mathbf{V}_{\text{noise}}(\boldsymbol{\alpha}_{\text{UV}}) \mathbf{K}^T \quad (57)$$

(noise in $n_{\text{H}_2\text{O}}$ is negligible). Here $\mathbf{V}_{\text{noise}}(\mathbf{B}^*)$ is a diagonal matrix containing the uncertainties given for the refractive increment in [11]. The reason to use $\mathbf{V} = \mathbf{V}_{\text{noise}}(\mathbf{y})$ is that the tensor-product structure (cf. Eq. (55) and Eq. (49)) of the systematic covariance matrices makes them singular and hence the full covariance matrix (including noise) close to singular, which is a problem for the numerics. But after all, weighting with uncertainties that arise from a global prefactor for all values has little sense.

Since $\hat{\mathbf{f}} = \mathbf{F} \mathbf{y}$ (Eq. (25)) is obtained by linear transformation, the covariance matrix is formally obtained as

$$\mathbf{V}_{\text{noise}}(\hat{\mathbf{f}}) = \mathbf{F} \mathbf{V} \mathbf{F}^T = \mathbf{H} (\mathbf{H}^T \mathbf{V}^{-1} \mathbf{H})^{-1} \mathbf{H}^T. \quad (58)$$

For the concentration contributions one obtains

$$\mathbf{V}_{\text{conc}}(\hat{\mathbf{f}}) = \sum_{j=1}^4 \mathbf{w}_j \mathbf{w}_j^T \quad \text{with} \quad \mathbf{w}_j = \mathbf{F} \mathbf{v}_j. \quad (59)$$

Although $\hat{\mathbf{f}}$ is formally the result of the fit, the quantity we are interested in is not $\hat{\mathbf{f}}$ but rather

$$\hat{\mathbf{B}} = \mathbf{B}_0 + \hat{\mathbf{f}} = \mathbf{B}_0 + \mathbf{F} \mathbf{y} = \mathbf{B}_0 + \mathbf{F} (\mathbf{B}^* - \mathbf{B}_0) = (\mathbf{F} - \mathbf{1}) \mathbf{B}_0 + \mathbf{F} \mathbf{B}^*, \quad (60)$$

where $\mathbf{1}$ denotes the identity matrix. We can assume \mathbf{B}^* (the measured refractive increment) and \mathbf{B}_0 (the part of the refractive increment computed from absorption spectra and water RI) to be uncorrelated and obtain we obtain

$$\begin{aligned} \mathbf{V}(\hat{\mathbf{B}}) &= (\mathbf{F} - \mathbf{1}) \mathbf{V}(\mathbf{B}_0) (\mathbf{F}^T - \mathbf{1}) + \mathbf{F} \mathbf{V}(\mathbf{B}^*) \mathbf{F}^T \\ &= \mathbf{V}(\mathbf{B}_0) + \mathbf{V}(\hat{\mathbf{f}}) - \mathbf{F} \mathbf{V}(\mathbf{B}_0) - \mathbf{V}(\mathbf{B}_0) \mathbf{F}^T. \end{aligned} \quad (61)$$

This also decomposes into

$$\mathbf{V}(\hat{\mathbf{B}}) = \mathbf{V}_{\text{noise}}(\hat{\mathbf{B}}) + \mathbf{V}_{\text{conc}}(\hat{\mathbf{B}}), \quad (62)$$

where both parts are computed separately. $\mathbf{V}_{\text{conc}}(\hat{\mathbf{B}})$ contributes stronger to the diagonal elements of $\mathbf{V}(\hat{\mathbf{B}})$ (i. e., the variances of the \hat{B}_i) than $\mathbf{V}_{\text{noise}}(\hat{\mathbf{B}})$. On the other hand, $\mathbf{V}_{\text{conc}}(\hat{\mathbf{B}})$ is strongly correlated among all elements, whereas $\mathbf{V}_{\text{noise}}(\hat{\mathbf{B}})$ is not. To illustrate the degree of correlation, the numerical derivative $B'(\lambda_i)$, obtained from finite differences, is plotted in Fig. 4 with the corresponding standard deviations.

D.1. Deoxyhemoglobin

The refractive increment for deoxyhemoglobin in Eq. (26) can also be written as

$$\mathbf{B}^{\text{deoxy}} = \mathbf{G}_{\text{lit}}^{\text{deoxy}} - \mathbf{F} \mathbf{G}_{\text{lit}} - (\mathbf{F} - \mathbf{1}) \mathbf{G}_{\text{H}_2\text{O}} + \mathbf{F} \mathbf{B}^*, \quad (63)$$

from which follows

$$\begin{aligned} \mathbf{V}_{\text{noise}}(\mathbf{B}^{\text{deoxy}}) &= \mathbf{V}_{\text{noise}}(\mathbf{G}_{\text{lit}}^{\text{deoxy}}) \\ &\quad + \mathbf{F} \mathbf{V}_{\text{noise}}(\mathbf{G}_{\text{lit}}) \mathbf{F}^T + \mathbf{F} \mathbf{V}_{\text{noise}}(\mathbf{B}^*) \mathbf{F}^T \end{aligned} \quad (64)$$

$$\mathbf{V}_{\text{conc}}(\mathbf{B}^{\text{deoxy}}) = \sum_{j=1}^6 \mathbf{u}_j \mathbf{u}_j^T \quad (65)$$

with

$$\begin{aligned} \mathbf{u}_j &:= \mathbf{F} \mathbf{v}_j \quad \text{for } j = 1, 2, 3; & \mathbf{u}_4 &:= (\mathbf{F} - \mathbf{1}) \mathbf{v}_4 \\ \mathbf{u}_5 &:= \sigma_{\text{conc,rel}} \mathbf{G}_{\text{VIS}}^{\text{deoxy}}, & \mathbf{u}_6 &:= \sigma_{\text{conc,rel}} \mathbf{G}_{\text{UV}}^{\text{deoxy}}. \end{aligned} \quad (66)$$

E. Peptide Absorption: Influence of Peak Shape

We have assumed the exact shape of the peptide peak to be of minor importance, such that the results depend mainly on its position, total strength and width. In order to justify this assumption quantitatively, we evaluated an alternative model, where the peak has a rectangular shape.

The comparison between results with the Lorentzian peak centered at $L = 187\text{ nm}$ and half width at half maximum $\Gamma = 11.6\text{ nm}$ and a rectangle centered around $L_{\text{II}} = L$ and half width $\Gamma_{\text{II}} = \Gamma$ reveals that deviations between the two models are negligible in comparison to the propagated data uncertainties for the majority of wavelengths. Only at wavelengths $\lambda < 400\text{ nm}$ does the deviation $|\hat{B}(\lambda) - \hat{B}_{\text{II}}(\lambda)|$ exceed the estimated uncertainties due to noise, but is still smaller than the total uncertainty including concentration errors. For $\lambda > 400\text{ nm}$ the deviation is at least one order of magnitude smaller than the total uncertainties.

ACKNOWLEDGMENT

The authors would like to thank Moritz Friebel for providing in tabulated form the absorbance data for oxygenated and deoxygenated hemoglobin published in [8] as figures.

REFERENCES

- R. Barer and S. Joseph, "Refractometry of living cells: Part I. basic principles," *Quarterly Journal of Microscopical Science* **s3-95**, 399–423 (1954).
- Y. Park, T. Yamauchi, W. Choi, R. Dasari, and M. S. Feld, "Spectroscopic phase microscopy for quantifying hemoglobin concentrations in intact red blood cells," *Opt. Lett.* **34**, 3668–3670 (2009).
- Y. Sung, N. Lue, B. Hamza, J. Martel, D. Irimia, R. R. Dasari, W. Choi, Z. Yaqoob, and P. So, "Three-dimensional holographic refractive-index measurement of continuously flowing cells in a microfluidic channel," *Physical Review Applied* **1**, 014002 (2014).
- E. Schonbrun, R. Malka, G. Di Caprio, D. Schaak, and J. M. Higgins, "Quantitative absorption cytometry for measuring red blood cell hemoglobin mass and volume," *Cytometry Part A* **85**, 332–338 (2014).
- Y. Kim, H. Shim, K. Kim, H. Park, S. Jang, and Y. Park, "Profiling individual human red blood cells using common-path diffraction optical tomography," *Scientific Reports* **4**, 6659 (2014).
- D. H. Tycko, M. H. Metz, E. A. Epstein, and A. Grinbaum, "Flow-cytometric light scattering measurement of red blood cell volume and hemoglobin concentration," *Applied Optics* **24**, 1355–1365 (1985).
- N. Mohandas, Y. R. Kim, D. H. Tycko, J. Orlik, J. Wyatt, and W. Groner, "Accurate And Independent Measurement Of Volume And Hemoglobin Concentration Of Individual Red-Cells By Laser-Light Scattering," *Blood* **68**, 506–513 (1986).
- M. Friebel and M. Meinke, "Determination of the complex refractive index of highly concentrated hemoglobin solutions using transmittance and reflectance measurements," *Journal of Biomedical Optics* **10**, 064019–064019–5 (2005).
- D. J. Faber, M. C. G. Aalders, E. G. Mik, B. A. Hooper, M. J. C. van Gemert, and T. G. van Leeuwen, "Oxygen saturation-dependent absorption and scattering of blood," *Physical Review Letters* **93**, 028102 (2004).
- O. Sydoruk, O. Zhernovaya, V. Tuchin, and A. Douplik, "Refractive index of solutions of human hemoglobin from the near-infrared to the ultraviolet range: Kramers-Kronig analysis," *Journal of Biomedical Optics* **17**, 115002–115002 (2012).
- M. Friebel and M. Meinke, "Model function to calculate the refractive index of native hemoglobin in the wavelength range of 250–1100 nm dependent on concentration," *Applied Optics* **45**, 2838–2842 (2006).
- H. J. Deuling and W. Helfrich, "Red blood cell shapes as explained on the basis of curvature elasticity," *Biophysical Journal* **16**, 861 (1976).
- V. Heinrich, K. Ritchie, N. Mohandas, and E. Evans, "Elastic thickness compressibility of the red cell membrane," *Biophysical Journal* **81**, 1452–1463 (2001).
- Y. Sugita, M. Nagai, and Y. Yoneyama, "Circular dichroism of hemoglobin in relation to the structure surrounding the heme," *Journal of Biological Chemistry* **246**, 383–388 (1971).
- S. Prahl, "Optical absorption of hemoglobin," <http://omlc.org/spectra/hemoglobin/> (1999).
- D. J. Segelstein, "The complex refractive index of water," Ph.D. thesis, University of Missouri – Kansas City (1981).
- G. Braunitzer, "The molecular weight of human haemoglobin." *Bibliotheca haematologica* **18**, 59 (1964).
- H. Arwin, "Optical properties of thin layers of bovine serum albumin, γ -globulin, and hemoglobin," *Applied Spectroscopy* **40**, 313–318 (1986).
- M. Daimon and A. Masumura, "Measurement of the refractive index of distilled water from the near-infrared region to the ultraviolet region," *Applied Optics* **46**, 3811–3820 (2007).
- A. R. Goldfarb, L. J. Saidel, and E. Mosovich, "The ultraviolet absorption spectra of proteins," *Journal of Biological Chemistry* **193**, 397–404 (1951).
- A. H. Woods and P. R. O'Bar, "Absorption of proteins and peptides in the far ultraviolet," *Science* **167**, 179–181 (1970).
- C. A. Emeis, L. J. Oosterhoff, and G. d. Vries, "Numerical evaluation of Kramers-Kronig relations," *Proceedings of the Royal Society of London. Series A, Mathematical and Physical Sciences* **297**, 54–65 (1967).
- L. H. Laasberg and J. Hedley-Whyte, "Optical rotatory dispersion of hemoglobin and polypeptides: Effect of halothane," *Journal of Biological Chemistry* **246**, 4886–4893 (1971).
- K. Witt, H. U. Wolf, C. Heuck, M. Kammel, A. Kummrow, and J. Neukammer, "Establishing traceability of photometric absorbance values for accurate measurements of the haemoglobin concentration in blood," *Metrologia* **50**, 539 (2013).